COMPARISON OF METHODS FOR CALCULATING THE RATE OF APPEARANCE OF EXOGENOUS GLUCOSE

by

Kai Bartlette

A thesis submitted to the Faculty and the Board of Trustees of the Colorado School of Mines in partial fulfillment of the requirements for the degree of Master of Science (Applied Mathematics).

Golden, Colorado

Date _____

Signed: _____
Kai Bartlette

Signed: _____
Cecilia Diniz Behn
Thesis Advisor

Golden, Colorado

Date _____

Signed: _____
Dr. Gregory Fasshauer
Professor and Head
Department of Applied Mathematics and Statistics

ABSTRACT

Insulin resistance (IR) is a crucial element of the pathology of the metabolic syndrome, which now affects more than a third of the population in the United States. Understanding the role of hepatic glucose release following a meal in contributing to hyperglycemia is crucial for the assessment of potential new medications. Using an oral glucose tolerance test (OGTT) protocol with two stable isotope tracers, both the rate of appearance of exogenous glucose (Ra_{exo}) coming from the drink and the suppression of endogenous glucose in response to the drink may be computed. In previous work, investigators have proposed several different methods for computing Ra_{exo}. The aim of this project was to compare the implementation and results of these methods applied to OGTT data from a cohort of obese adolescent girls. Methods were compared based on inter-method variability and known physiology. Obtaining a reliable estimate of the rate of appearance of exogenous glucose from the drink is necessary to assess hepatic IR. In addition, such an estimate represents a key input to differential equations-based models of whole body glucose-insulin dynamics that are used to quantify hepatic IR, and the method-dependence of the resulting estimates of insulin sensitivity has not been assessed. Improved understanding of interactions between exogenous and endogenous hepatic glucose dynamics will facilitate the characterization of IR in individual patients and different disease conditions and may support the development of targeted therapeutic approaches.

TABLE OF CONTENTS

LIST OF FIGURES

LIST OF TABLES

LIST OF ABBREVIATIONS

Rate of appearance of glucose	Ra
Rate of appearance of exogenous glucose	Ra_{exo}
Rate of appearance of endogenous glucose	Ra_{endo}
Oral Glucose Tolerance Test	OGTT
Intravenous Glucose Tolerance Test	IVGTT
Insulin Resistance	IR
Insulin Sensitivity	S_I
Oral Minimal Model	OMM
Labeled Oral Minimal Model	OMM*
Reference Model	RM
Reference-Labeled Model	RM*
Final Model	FM
Tracer-to-Tracee Ratio	TTR

CHAPTER 1
INTRODUCTION

The maintenance of blood glucose is chiefly regulated by the liver and pancreas and is necessary to provide a constant energy supply of glucose for the brain. While fasting, endogenous glucose is released from the liver into the blood. In the postprandial state, the pancreas releases insulin in response to elevated glucose levels to signal the liver and other tissues to take up glucose. The appearance of exogenous glucose leads to the suppression of endogenous glucose production [16]. The regulation of blood glucose is an important metabolic process that, when impaired, can lead to a wide variety of health issues and diseases. A better understanding of this complex system is needed to support the development of therapeutic approaches.

The dynamics of exogenous glucose reflect absorption and uptake of glucose from the blood glucose pool. Dynamics of endogenous glucose reflect hepatic glucose production. To gather insight on glucose kinetics following a meal, an oral glucose tolerance test (OGTT) protocol with two stable isotope glucose tracers was used in a cohort of obese adolescent females. During the protocol, blood samples were collected at regular intervals and gas chromatography mass spectrometry was used to measure relative abundance of glucose tracers and tracee. The ratios of tracer to tracee were used to calculate the total rate of appearance of glucose (Ra), the appearance of exogenous glucose (Ra_{exo}) and the rate of appearance of endogenous glucose (Ra_{endo}).

Total Ra represents the rate of appearance of glucose due to both endogenous and exogenous glucose contributions. Investigators have provided various methods of computing Ra_{exo}. Ra_{endo} is defined to be the difference of total Ra and Ra_{exo}. This project focuses

on comparing the implementation and results of four methods for calculating Ra_{exo}. An estimate of Ra_{exo} is a key input to differential equation based models of glucose-insulin dynamics but the method-dependence of these implementations has not, to our knowledge, been systematically investigated. Each method will be thoroughly motivated and derived. Following implementation, method-dependence of the simulated glucose-insulin dynamics and estimates of insulin sensitivity will be assessed.

A detailed description of the regulation of blood glucose and the models developed to describe glucose kinetics follows in the next chapter. The motivating differential equation based models for this project are described, followed by the full description of the data and protocol performed. The methods for computing Ra_{exo} will be fully derived followed by a description of their implementation into the motivating models. Implementations and results will be discussed.

CHAPTER 2

BACKGROUND

Glucose homeostasis is a complex metabolic process by which the body maintains blood glucose levels within a narrow margin. Regulation is primarily controlled by the liver, pancreas and to a lesser extent the kidneys. In healthy fasting adults, blood glucose concentrations range primarily from 3.5 to 6.0 $mmol \cdot l^{-1}$ and rarely exceed 11 $mmol \cdot l^{-1}$ in arterial blood or 10 $mmol \cdot l^{-1}$ in venous blood [16]. Following a meal, exogenous glucose enters the blood through gut absorption. The increased blood glucose levels prompt the release of insulin and the suppression of glucagon secretion by the pancreas. With more insulin circulating, insulin-sensitive peripheral tissues such as adipose, muscle, and skin are able to take in glucose from the blood at an accelerated rate. The reduced production of the hormone glucagon in the blood signals the liver to reduce the amount of glucose it releases and to increase uptake of glucose to be stored in its polymeric form known as glycogen. During the fasted state, insulin levels are low and no longer inhibit glucagon production. Increased glucagon signals the liver to break down stored glycogen to be released as glucose into the bloodstream. Also, to a lesser extent, the kidneys make new glucose to be released. This keeps glucose levels from being too low when fasting [16].

Insulin plays a major role in glucose homeostasis. It is the main hormone able to lower blood glucose levels by promoting glucose uptake and inhibiting endogenous glucose production [16]. When the metabolic response to insulin is impaired, insulin-sensitive tissues fail to respond to ordinary levels of insulin circulating in the blood [2]. This insulin resistance (IR) means that more insulin than previously needed is required to reduce the amount of glucose in the blood. IR is a risk factor for many metabolic diseases and syndromes such as type 2 diabetes mellitus, polycystic ovarian syndrome and cardiovascular disease. IR affects

approximately 10 - 25% of the population and the risk increases in obese individuals [2]. This project focused on assessing IR in obese adolescent girls. Previous studies have shown that IR increases in adolescents, especially in adolescent girls [17].

Over several decades, models have been developed to describe glucose kinetics in humans ranging in complexity. Some have been developed to analyze whole body glucose regulation by including compartments to account for glucose absorption in the gastrointestinal tract and the effect of incretin production on pancreatic insulin production in addition to sub-models that describe glucose, insulin and glucagon concentrations [21]. In a different direction, models have been developed to examine β-cell function and mass to compensate for an increased demand of insulin [9]. A deeper understanding of this important metabolic process leads to more targeted treatments.

The widely used Minimal Model (MM) for an intravenous glucose tolerance test (IVGTT) uses a system of differential equations to describe glucose and insulin action [6]. A ratio of two of the parameters of this model defines an insulin sensitivity index (S_I) that quantifies the ability of insulin to suppress glucose production and promote glucose disposal [6, 12, 13, 14]. Extensions and alterations have been made to this model to describe glucose kinetics in a physiological context. The Oral Minimal Model (OMM) has a similar structure to the MM but has additional functions to account for an oral glucose load. This model describes total glucose dynamics during an OGTT or following a meal [12]. Solely to describe the dynamics of meal glucose, the Labeled Oral Minimal Model (OMM*) was developed [13]. These models will be discussed in more detail in Chapter 3 as the main motivation for this project.

CHAPTER 3

MOTIVATION

The motivation for this comparison of methods for computing exogenous glucose is investigating method-dependence of simulated glucose-insulin dynamics and predictions of insulin sensitivity using the Oral Minimal Model (OMM) and the Labeled Oral Minimal Model (OMM*). These models describe glucose dynamics after an OGTT or a meal. They are a coupling of the MM with a parametric description of the rate of appearance of orally administered glucose, Ra_{exo} [14]. Ra_{exo} is assumed to be unknown and the governing parameters are estimated using least squares. The model is represented by the following equations:

$$\begin{cases} \dot{G}(t) = -[S_G + X(t)] \cdot G(t) + S_G \cdot G_b + \frac{Ra_{meal}(\boldsymbol{\alpha},t)}{V}, & G(0) = G_b \\ \dot{X}(t) = -p_2 \cdot X(t) + p_3 \cdot [I(t) - I_b], & X(0) = 0 \end{cases} \tag{3.1}$$

with

$$Ra_{meal}(\boldsymbol{\alpha}, t) = \begin{cases} \alpha_{i-1} + \frac{\alpha_i - \alpha_{i-1}}{t_i - t_{i-1}}(t - t_{i-1}), & \text{for } t_{i-1} \le t \le t_i \quad i = 1, \ldots, n \\ 0, & \text{otherwise} \end{cases} \tag{3.2}$$

where $\boldsymbol{\alpha}$ denotes $[\alpha_1, \alpha_2, \ldots, \alpha_n]^T$, $G(t)$ is glucose concentration, $X(t)$ is insulin action on glucose absorption and production, $I(t)$ is insulin concentration in plasma, V is the volume of distribution, G_b and I_b represent basal values of glucose and insulin, respectively, and S_G, p_2, and p_3 are rate parameters. By definition, S_G is the fractional glucose effectiveness measuring the ability of glucose to promote glucose absorption and inhibit glucose production; p_2 is the constant rate parameter that describes the dynamics of the decay of insulin action and p_3 controls the amplitude of insulin action response to the difference between insulin and baseline insulin concentrations [12, 13, 14]. The developers of this model came to the conclusion that this piecewise-linear description of Ra_{meal} is superior to a spline or dynamic model. It is the simplest and does not assume a specific functional form of Ra_{meal} [14].

OMM* has a similar structure to OMM and both have the same exogenous glucose input $Ra_{meal}(\boldsymbol{\alpha}, t)$:

$$\begin{cases} \dot{G}_{meal}(t) = -[S_G^* + X^*(t)] \cdot G_{meal}(t) + \frac{Ra_{meal}(\boldsymbol{\alpha},t)}{V^*}, & G_{meal}(0) = 0 \\ \dot{X}^*(t) = -p_2^* \cdot X^*(t) + p_3^* \cdot [I(t) - I_b], & X^*(0) = 0 \end{cases} \tag{3.3}$$

where S_G^* is the fractional glucose effectiveness measuring the ability of glucose to promote glucose absorption, $X^*(t)$ is insulin action on glucose absorption, p_2^* and p_3^* are rate constants describing the dynamics and magnitude of $X(t)$, respectively [13].

From these models, an S_I index reflecting the ability of insulin to suppress glucose production and promote glucose uptake can be computed. The S_I index calculated using OMM measures the ability of insulin to both suppress glucose production and promote glucose uptake in the postprandial state [12, 14]. This composite index is not able to quantify insulin's ability to solely enhance glucose disposal. Theoretically, the disappearance of a labeled glucose could track ingested glucose disposal. Using the parameters from OMM*, the S_I^* index reflects the ability of insulin to promote glucose disposal [13]. In terms of the model parameters, S_I and S_I^* are given by

$$S_I = \frac{p_3}{p_2} \cdot V \tag{3.4}$$

$$S_I^* = \frac{p_3^*}{p_2^*} \cdot V \tag{3.5}$$

where S_I and S_I^* have units $mL \cdot kg^{-1} \cdot min^{-1}$ per $\mu U \cdot mL^{-1}$ [13]. The ratio of these parameters define measures of insulin sensitivity because they involve the parameters that govern the rate and amplitude of insulin acting on glucose.

In these models, the parameters to be estimated are S_G, p_2, p_3, V, S_G^*, p_2^*, p_3^*, V^* and $\boldsymbol{\alpha}$. Previous work has established that these models are structurally unidentifiable thus every

parameter cannot be uniquely estimated [13]. More specifically, parameters from the ratio of $\boldsymbol{\alpha}/V$ and $\boldsymbol{\alpha}/V^*$ cannot be uniquely identified. To overcome this problem, a two step process involving three identifiable sub-models are used: the Reference Model (RM) for total glucose, the Reference-Labeled Model (RM*) for meal glucose [12, 13], and the Final Model (FM). In RM and RM*, the rate of appearance of exogenous glucose is calculated from the data to provide a reference $Ra^{ref}_{meal}(t)$ in which the $\alpha_i, i = 0, \ldots, n$ are fixed. RM is given by

$$\begin{cases} \dot{G}(t) = -[S_G^{ref} + X^{ref}(t)] \cdot G(t) + S_G^{ref} \cdot G_b + \frac{Ra^{ref}_{meal}(t)}{V^{ref}}, & G(0) = G_b \\ \dot{X}^{ref}(t) = -p_2^{ref} \cdot X^{ref}(t) + p_3^{ref} \cdot [I(t) - I_b], & X^{ref}(0) = 0 \end{cases} \tag{3.6}$$

and RM* is given by

$$\begin{cases} \dot{G}_{meal}(t) = -[S_G^{*ref} + X^{*ref}(t)] \cdot G_{meal}(t) + \frac{Ra^{ref}_{meal}(t)}{V^{*ref}}, & G_{meal}(0) = 0 \\ \dot{X}^{*ref}(t) = -p_2^{*ref} \cdot X^{*ref}(t) + p_3^{*ref} \cdot [I(t) - I_b], & X^{*ref}(0) = 0 \end{cases}. \tag{3.7}$$

Letting $Ra^{ref}_{meal}(t) = Ra_{exo}$ requires a reliable method for calculating Ra_{exo} from data. Once an estimate for $Ra^{ref}_{meal}(t)$ is calculated, the remaining parameters are estimated using RM and RM*. From RM and RM*, S_I^{ref} and S_I^{*ref} indices can be calculated. With the estimated parameters fixed in the FM, the $\alpha_i, \ldots, \alpha_n$ can be estimated. The parameters from FM are used to compute S_I and S_I^*. Since Ra_{meal} is fixed in the beginning of this two step process, different Ra_{meal} estimates may affect estimates of S_I and S_I^*.

CHAPTER 4

DATA AND PROTOCOL

Participants were recruited from pediatric clinics at the Children's Hospital Colorado to complete an OGTT with stable isotope tracers. They included obese girls (BMI $\geq$ 95th percentile for age) without type 2 diabetes. All were sedentary (less than 3 hours per week of exercise, verified by standardized 3-day activity recall, and 7-day accelerometer recording, Actigraph, Pensacola, FL) and had achieved Tanner Stage 5 in puberty [1] (as assessed by physical exam by a pediatric endocrinologist, Kristen J. Nadeau or Melanie Cree-Green). Prior to the study, anemia was ruled out in all subjects. Exclusionary medications included antihypertensives, lipid lowering agents, oral steroids, atypical antipsychotics and metformin. This study was approved by the University of Colorado Anschutz Medical Campus Institutional Review Board and the Children's Hospital of Colorado Scientific Advisory Review Committee. Parental informed consent and participant assent was obtained from all participants less than 18 years old and participant consent from those aged 18 years and above.

Three days before the overnight stay, participants consumed 3 days of an isocaloric diet (55 % carbohydrate, 15% protein, 30% fat) and refrained from physical activity. The tracer infusion protocol began with baseline blood samples (for background enrichment of glucose and concentrations of glucose and insulin) taken at approximately 6 AM then a constant infusion of glucose stable isotope began. A bolus of 24.97 $Umol \cdot kg^{-1}$ $[6,6\text{-}^2H_2]$ glucose (tracer II, Isotex, Miamisville, IA) was given. Then $[6,6\text{-}^2H_2]$ glucose was intravenously infused at a constant rate of 0.2222 $Umol \cdot kg^{-1} \cdot min^{-1}$ continually throughout the study. Starting at 7:30 AM, blood was sampled 4 times, each 10 minutes apart, for glucose and insulin concentrations and to assure basal glucose tracer enrichment values [8] then the

[1] The Tanner Scale is a scale of pubertal development in children and adolescents based on external primary and secondary sex characteristics. Tanner Stage 5 is the final stage.

subjects received a sugary drink (Glucola) containing a standard 75 grams of glucose with an additional 222.02 $Umol \cdot kg^{-1}$ of [1-^{13}C] glucose (tracer I). Blood samples were collected initially every 10 minutes for 30 minutes then every 15 minutes for 2 hours then every 30 minutes for 2 hours then every hour until the end of the study. Previous knowledge of plasma glucose rate of appearance following ingestion suggests that glucose changes rapidly following drink ingestion and then changes more slowly as it recovers baseline values. To more accurately capture the initial appearance of exogenous Ra, measurements were sampled more frequently in the beginning of the protocol and less frequently towards the end.

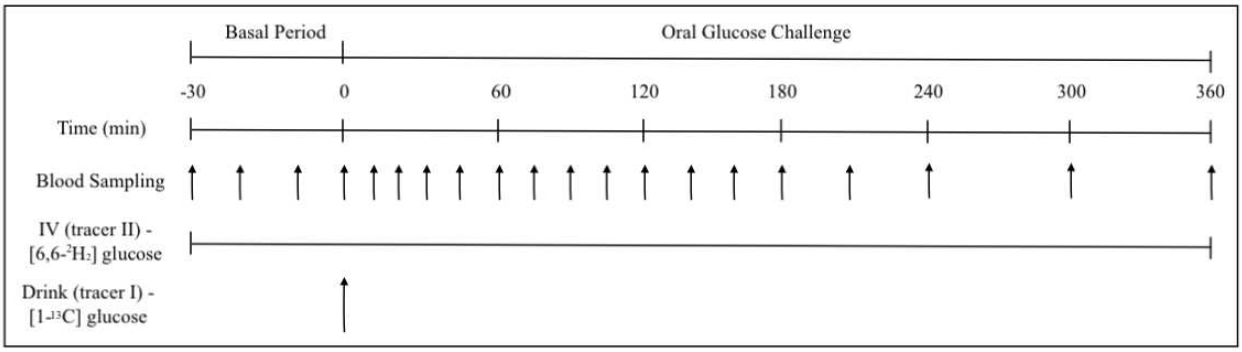

Figure 4.1: OGTT protocol timeline where subjects had glucose tracer II intravenously infused and ingested glucose tracer I

Samples for plasma glucose were analyzed using a modification of the negative ion chemical ionization gas chromatography mass spectrometry [8, 5, 4]. The 331, 332 and 333 fragments produced by chemical ionization were measured [22]. Fragment 331 corresponds to glucose tracee, 332 to glucose tracer I and 333 to glucose tracer II. Blood glucose concentrations were found using modified glucose oxidase-based method on a StatStrip®hospital glucose monitoring system (Nova Biomedical, Waltham, MA), which has been previously demonstrated to be equivalent with with a YSI 2300 STAT Plus™(YSI, Inc, Yellow Springs, OH) glucose analyzer [11]. Serum insulin concentration was determined with radioimmunoassay (Millipore, Billerica, MA).

The ratios of tracer I and tracer II to tracee were used to track changes in relative enrichment. Relative abundance of each tracer is reported as tracer-to-tracee ratio (TTR). The raw tracer data was corrected to account for the patients' background enrichments and glucose isotopes coming from other sources. The corrections for [1-^{13}C] glucose tracer I were computed as follows:

- Compute TTR of tracer I to tracee using raw counts.
- Subtract 6 am value to correct for patient's background.
- Subtract average of 6 am to 8 am values to correct for [1-^{13}C] glucose coming from the IV.
- Multiply by (1-0.011) for skew correction.

For [6, 6-$^{2}H_2$] glucose tracer II, the corrections were computed as follows:

- Compute TTR of tracer II to tracee using raw counts.
- Subtract 6 am value to correct for patient's background.
- Multiply the skew corrected measurement of tracer I by the proportion of tracer II to tracer I in the drink to compute the amount of [6, 6-$^{2}H_2$] glucose tracer II coming from the drink.
- Subtract [6, 6-$^{2}H_2$] glucose tracer II coming from the drink.

The corrected tracer data was used to compute total and exogenous rate of appearance of glucose as described in Chapter 5.

CHAPTER 5

METHODS

In the following section, we take an in depth look into the derivations and implementation of each of the published methods for computing the rate of appearance of exogenous glucose. To begin, we start by calculating Steele's non-steady state model for total rate of appearance of glucose.

5.1 Steele's Non-Steady State Ra

Each of the following methods for calculating Ra_{exo} are based on Steele's non-steady state model for total Ra. We use the mass balance equations for total glucose and tracer II to determine the rate of appearance of total glucose, Ra:

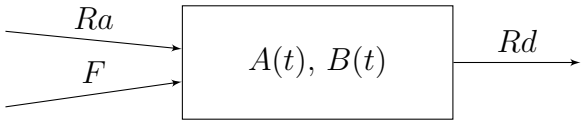

Figure 5.1: Schematic of glucose kinetics where Ra is the total rate of appearance of glucose, F is the infusion rate of glucose tracer, Rd is the rate of disappearance of glucose, $A(t)$ is the amount of tracer II and $B(t)$ is the amount of tracee.

In Figure 5.1, let Ra denote the rate of appearance of glucose, F be the infusion rate of the tracer II and Rd be the rate of disappearance of glucose. Define $A(t)$ and $B(t)$ as the amount of tracer II and tracee, respectively, at time t. Then $E(t)$, defined as $E(t) = \frac{A(t)}{B(t)}$, is the tracer-to-tracee ratio (TTR) of the plasma at time t. Then,

$$A(t) = B(t)E(t) \tag{5.1}$$

$$\frac{dA(t)}{dt} = B(t)\frac{dE(t)}{dt} + E(t)\frac{dB(t)}{dt} \tag{5.2}$$

The rate of change of tracee in the plasma is the rate in of tracee minus the rate out:

$$\frac{dB(t)}{dt} = Ra - Rd. \tag{5.3}$$

An analogous formula may be used to describe the rate of change of tracer II. However, since tracer II is constantly infused, $Ra_{2H} = F$ so the rate of change of tracer II is the infusion rate minus $E(t) \cdot Rd$,

$$\begin{aligned} \frac{dA(t)}{dt} &= Ra_{2H} - Rd_{2H} \\ &= F - \frac{A(t)}{B(t)} Rd \\ &= F - E(t)Rd \end{aligned} \tag{5.4}$$

Combining equations 5.2, 5.3 and 5.4 we obtain the following formula for total Ra:

$$Ra - Rd = \frac{\frac{A(t)}{dt} - B(t)\frac{E(t)}{dt}}{E(t)} \tag{5.5}$$

$$\implies Ra = \frac{F - E(t)Rd - B(t)\frac{dE(t)}{dt}}{E(t)} + Rd \tag{5.6}$$

$$\implies Ra = \frac{F - B(t)\frac{dE(t)}{dt}}{E(t)} - \cancel{\frac{E(t)Rd}{E(t)}} + \cancel{Rd} \tag{5.7}$$

$$\implies Ra = \frac{F - B(t)\frac{dE(t)}{dt}}{E(t)} \tag{5.8}$$

Here, the entire glucose pool is regarded as a single compartment. To account for imperfect mixing of glucose throughout the pool, Steele introduces the pool fraction, p, to represent the fraction of the glucose pool that is rapidly mixing. Then we can rewrite $B(t)$ as $B(t) = pVC(t)$, where V is the volume of the glucose pool and $C(t)$ is the concentration of glucose at time t. Hence, pV represents the volume of distribution for glucose. Thus, Steele's equation for non-steady state Ra is written as

$$Ra = \frac{F - pV\,C(t)\,\frac{dE(t)}{dt}}{E(t)}. \tag{5.9}$$

In calculations, Ra is approximated using the following formula

$$Ra = \frac{F - pV[(C_2 + C_1)/2] \cdot [(E_2 - E_1)/(t_2 - t_1)]}{[(E_2 + E_1)/2]} \tag{5.10}$$

where the (t) notation has been suppressed, C_1 and C_2 are plasma glucose concentrations at times t_1 and t_2, respectively; E_1 and E_2 are plasma TTR of tracer II to tracee at times t_1 and t_2, respectively [20, 10].

5.2 Exogenous Ra

Steele's equation represents appearance of glucose in the blood from both endogenous and exogenous sources. Endogenous glucose is produced mainly by the liver, and exogenous glucose comes from a meal. The following sections outline the various methods for calculating the rate of appearance of ingested glucose.

5.2.1 Clamp Model

This method calculates Ra_{exo} by scaling total Ra by the normalized enrichment of tracer I. Total Ra is calculated using tracer II and Steele's formula. Then the total Ra is scaled by the ratio of the enrichment of tracer I in the plasma to the enrichment of tracer I in the test drink [10].

$$Ra_{exo} = Ra\left(\frac{E_P}{E_D}\right) \tag{5.11}$$

where E_D and E_P are the enrichments of [1-^{13}C] glucose from the test drink and plasma, respectively. The aim of scaling total Ra by this ratio is to calculate the proportion of glucose appearance coming from an exogenous source.

5.2.2 One Pool Model

This method calculates Ra_{exo} by solving for the variable infusion rate of ingested glucose and then scaling this by the enrichment of tracer I in the drink. Known total Ra and Steele's non-steady state equation are used with tracer I to solve for the variable infusion rate, due to gut absorption dynamics, of tracer I, [18] Ra_{13C}. Theoretically, total Ra should be the same

if computed with tracer I or tracer II. Tracer II is used in calculations of total Ra because the infusion rate of tracer II is known. Ra_{13C}, is scaled by the enrichment of tracer I in the drink to compute Ra_{exo}. To solve for Ra_{13C}, consider Steele's equation 5.9 in terms of tracer I where F is replaced with Ra_{13C} to represent the infusion rate of tracer I:

$$Ra = \frac{Ra_{13C} - pVC\frac{dE}{dt}}{E}.$$

Then solve for Ra_{13C}

$$Ra_{13C} = Ra \cdot E + pV \cdot C \cdot \frac{dE}{dt} \tag{5.12}$$

and scale by the enrichment of the drink to obtain

$$Ra_{exo} = \frac{Ra_{13C}}{E_D}. \tag{5.13}$$

5.2.3 One Compartment Model

Figure 5.2: Schematic showing change in tracers in one compartment where Ra_{13C} is the rate of appearance of tracer I, F_{2H} is the infusion rate of tracer II and G is the accessible compartment of each tracer.

This method computes Ra_{exo} by applying Steele's equation to estimated concentrations of [1-^{13}C] glucose. It assumes one accessible compartment from which Ra and Rd, rate of appearance and disappearance, respectively, occur and where glucose tracers are measured (see Figure 5.2) [3]. The product pV represents the rapidly mixing compartment in which the mass balance equations for the [6, 6-$^2H_2$] glucose tracer imply

$$pV\frac{dG_{2H}}{dt} = F_{2H} - Rd_{2H} \tag{5.14}$$

where G_{2H} is the concentration of [6, 6-$^2H_2$] glucose tracer in plasma, F_{2H} is the rate of infusion and Rd_{2H} is the rate of disappearance in plasma.

Similarly, for the [1-^{13}C] glucose tracer

$$pV\frac{dG_{13C}}{dt} = Ra_{13C} - Rd_{13C} \tag{5.15}$$

where G_{13C} is the concentration of [1-^{13}C] glucose tracer in plasma, and Ra_{13C} and Rd_{13C} are the rate of appearance of [1-^{13}C] glucose tracer and disappearance in plasma, respectively.

The indistinguishability of the isotope tracers yields the following relationship that links the disappearance rate of the two glucose tracers

$$\frac{Rd_{13C}}{pVG_{13C}} = \frac{R_{2H}}{pVG_{2H}} = k_{01} \tag{5.16}$$

where k_{01} is the disappearance rate parameter, assumed to vary during the experiment. Using 5.16, rewrite 5.14 and 5.15 as

$$pV\frac{dG_{2H}}{dt} = F_{2H} - k_{01}\, pV\, G_{2H} \tag{5.17}$$

$$pV\frac{dG_{13C}}{dt} = Ra_{13_C} - k_{01}pVG_{13C}. \tag{5.18}$$

Solve 5.17 for k_{01} as

$$k_{01} = \frac{F_{2H}}{pVG_{2H}} - \frac{dG_{2H}/dt}{G_{2H}}. \tag{5.19}$$

Plugging 5.19 into 5.18 to arrive at an expression for Ra_{13C}:

$$\begin{aligned} Ra_{13C} &= pV\frac{dG_{13C}}{dt} + k_{01}pVG_{13C} \\ &= pV\frac{dG_{13C}}{dt} + \left(\frac{F_{2H}}{pVG_{2H}} - \frac{dG_{2H}/dt}{G_{2H}}\right) pVG_{13C} \\ &= \frac{F_{2H}}{G_{2H}/G_{13C}} + pV\frac{dG_{13_C}}{dt} - \frac{pV}{G_{2H}/G_{13C}}\frac{dG_{2H}/dt}{G_{2H}}. \end{aligned}$$

Using the relationship

$$\frac{d}{dt}\Big(\frac{G_{2H}}{G_{13\,C}}\Big) = \frac{G_{13\,C}\frac{dG_{2H}}{dt} - G_{2H}\frac{dG_{13\,C}}{dt}}{(G_{13\,C})^2} = \frac{1}{G_{13\,C}}\frac{dG_{2H}}{dt} - \frac{G_{2H}}{{G_{13\,C}}^2}\frac{dG_{13\,C}}{dt},$$

the following expression for Ra_{13C} is found:

$$\begin{aligned} Ra_{13C} &= \frac{F_{2H}}{G_{2H}/G_{13C}} - pV\Big(\frac{1}{G_{2H}/G_{13C}}\frac{dG_{2H}}{dt} - \frac{dG_{13_C}}{dt}\Big) \\ &= \frac{F_{2H}}{G_{2H}/G_{13C}} - pV\Big(\frac{1}{G_{2H}/G_{13\,C}}\frac{dG_{2H}}{dt} - \frac{dG_{13_C}}{dt}\Big)\Big(\frac{G_{2H}}{G_{2H}}\Big)\Big(\frac{G_{13\,C}}{G_{13\,C}}\Big)^2 \\ &= \frac{F_{2H}}{G_{2H}/G_{13C}} - pV\Big(\frac{{G_{13C}}^2}{G_{2H}}\Big)\Big(\frac{1}{G_{13C}}\frac{dG_{2H}}{dt} - \frac{G_{2H}}{{G_{13C}}^2}\frac{dG_{13C}}{dt}\Big) \end{aligned}$$

$$Ra_{13C} = \frac{F_{2H}}{G_{2H}/G_{13C}} - \frac{pVG_{13C}}{G_{2H}/G_{13C}}\Big(\frac{d(G_{2H}/G_{13C})}{dt}\Big) \tag{5.20}$$

This formula for Ra_{13C} is then scaled by the enrichment of the drink:

$$Ra_{exo} = \frac{Ra_{13C}}{E_D}. \tag{5.21}$$

5.2.4 Two Compartment Model

This model computes Ra_{exo} by applying Steele's equation to estimated concentrations of [1-^{13}C] glucose and additionally considering exchange between a remote and an accessible compartment for the glucose pool. The assumed two-compartment system has a time-varying disappearance rate from the accessible compartment, k_{01}, and constant rate parameters between the accessible and peripheral compartments k_{21} and k_{12} [3]. For glucose flow of the two tracers used in the protocol see Figure 5.3.

From the mass balance equations for each isotope (see Figure 5.3) we have

$$V_1\frac{dG_{2H}}{dt} = F_{2H} - (k_{01} + k_{21})V_1G_{2H} + k_{12}Q_{2H} \tag{5.22}$$

$$V_1\frac{dG_{13C}}{dt} = Ra_{13C} - (k_{01} + k_{21})V_1G_{13C} + k_{12}Q_{13C}, \tag{5.23}$$

where V_1 is the volume of the accessible compartment, and Q_{2H} and Q_{13C} are the amounts of [6, 6-$^2H_2$] and [1-^{13}C] glucose, respectively, in the peripheral compartments. We can derive a formula for k_{01} using 5.22 to yield

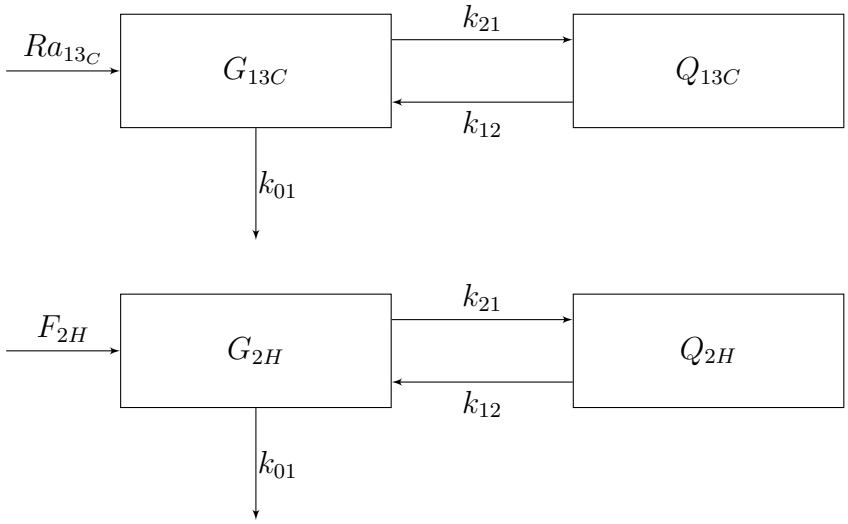

Figure 5.3: Schematic showing change in tracers in two compartments where Ra_{13C} is the rate of appearance of tracer I, F_{2H} is the infusion rate of tracer II, k_{12}, k_{21} and k_{01} are rate parameters, G and Q are the accessible and remote compartments, respectively, of each tracer.

$$\begin{aligned} k_{01} &= \frac{V_1 \frac{dG_{2H}}{dt} - F_{2H} - k_{12}Q_{2H}}{-V_1 G_{2H}} - k_{21} \\ &= \frac{F_{2H}}{V_1 G_{2H}} + \frac{k_{12}Q_{2H}}{V_1 G_{2H}} - \frac{1}{G_{2H}}\frac{dG_{2H}}{dt} - k_{21}. \end{aligned} \tag{5.24}$$

Using 5.24 in 5.23 the following expression for Ra_{13C} is found.

$$\begin{aligned} V_1\frac{dG_{13C}}{dt} &= Ra_{13_C} - \left(\frac{F_{2H}}{V_1 G_{2H}} + \frac{k_{12}Q_{3H}}{V_1 G_{2H}} - \frac{1}{G_{2H}}\frac{dG_{2H}}{dt}\right) V_1 G_{13C} + k_{12}Q_{13_C} \\ Ra_{13_C} &= \frac{F_{2H}}{G_{2H}/G_{13C}} + V_1\frac{dG_{13C}}{dt} + \frac{V_1}{G_{2H}/G_{13C}}\frac{dG_{2H}}{dt} + k_{12}\left(\frac{Q_{2_H}}{G_{2H}/G_{13C}} - Q_{13_C}\right) \\ &= \frac{F_{2H}}{G_{2H}/G_{13C}} - \Big(\frac{V_1 G_{13\,C}^2}{G_{2H}}\Big)\Big(\frac{1}{G_{13\,C}}\frac{dG_{2H}}{dt} - \frac{G_{2H}}{{G_{13\,C}}^2}\frac{dG_{13\,C}}{dt}\Big) + k_{12}\left(\frac{Q_{2_H}}{G_{2H}/G_{13C}} - Q_{13_C}\right) \end{aligned}$$

$$Ra_{13_C} = \frac{F_{2H}}{G_{2H}/G_{13C}} - \frac{V_1 G_{13\,C}}{G_{2H}/G_{13\,C}}\Big(\frac{d(G_{2H}/G_{13\,C})}{dt}\Big) + k_{12}\left(\frac{Q_{2_H}}{G_{2H}/G_{13C}} - Q_{13C}\right) \tag{5.25}$$

Then Ra_{exo} is computed as

$$Ra_{exo} = \frac{Ra_{13C}}{E_D}. \tag{5.26}$$

The equations describing the amount of each tracer in the peripheral compartment were derived from the mass balance equations as

$$\frac{dQ_{2H}}{dt} = -k_{12}Q_{2H} + k_{21}V_1G_{2H} \tag{5.27}$$

$$\frac{dQ_{13C}}{dt} = -k_{12}Q_{13C} + k_{21}V_1G_{13C}. \tag{5.28}$$

The third term of 5.25 was computed iteratively using the calculation scheme below. This method required Ra_{exo} to be calculated over equally spaced time intervals. To utilize this approach, the OGTT data for each subject was interpolated with each time interval equal to 10 minutes. Let $R_2(t)$ denote the third term to be calculated using the following equations:

$$R_2(t_k) = V_2k_{12}\left[\frac{g^*(t_k)}{G_{2H}(t_k)/G_{13C}(t_k)} - g(t_k)\right] \tag{5.29a}$$

$$g(t_{k+1}) = b_1g(t_k) + b_2G_{2H}(t_k) + b_3G_{2H}(t_{k+1}) \tag{5.29b}$$

$$g^*(t_{k+1}) = b_1g^*(t_k) + b_2G_{13C}(t_k) + b_3G_{13C}(t_{k+1}) \tag{5.29c}$$

$$g(t_0) = G_{2H}(t_0) \qquad g^*(t_0) = G_{13C}(t_0) \tag{5.29d}$$

$$b_1 = e^{-k_{12}T} \tag{5.29e}$$

$$b_2 = \frac{1-b_1}{k_{12}T} - b_1 \tag{5.29f}$$

$$b_3 = 1 - \frac{1-b_1}{k_{12}T}. \tag{5.29g}$$

$R_2(t_k), g(t_k)$ and $g^*(t_k)$ are calculated at the discrete time points over the whole time interval of the OGTT protocol. Initially, $R_2(t_0) = 0$ and $g(t_k)$ and $g^*(t_k)$ are updated to calculate the next step of $R_2(t_k)$. The parameters b_1, b_2 and b_3 are constant, V_2 is the volume of the remote compartment and $T = 10$ minutes is the time interval between each time point [15].

5.3 Implementation into OMM/OMM*

Once the Ra_{exo} methods have been computed, sensitivity of OMM and OMM* to each method can be analyzed. To begin, an estimate of Ra_{exo} from a chosen method was fixed in RM for total glucose and RM* for meal glucose as Ra_{meal}^{ref}. Parameters S_G^{ref}, p_2^{ref}, p_3^{ref}, V^{ref}, S_G^{*ref}, p_2^{*ref}, p_3^{*ref} and V^{*ref} were estimated using least squares. These reference parameter estimates were used to fix S_G, S_G^*, V and V^* in FM. This allows unique estimation of the α_i, $i = 0, \ldots, n$ in $Ra_{meal}(\boldsymbol{\alpha}, t)$ as well as the parameters p_2, p_3, p_2^* and p_3^*. Then the parameters from FM were used to compute S_I and S_I^*. Since the Ra_{meal} parameters are estimated in FM, the methods used to compute Ra_{meal} are an intermediate step in the process used to estimate insulin sensitivity. This raises the issue of the sensitivity of the estimated values of S_I and S_I^* to the chosen method of estimating Ra_{exo}.

CHAPTER 6

RESULTS

For each subject (n = 3), we computed Ra_{exo} using each method and implemented these forms of Ra_{exo} into RM and RM*. We report glucose and insulin data, Steele's Ra, Ra_{exo} and Ra_{endo} for all the methods, and the results of the implementation of the Ra_{exo} methods into RM and RM* for all subjects.

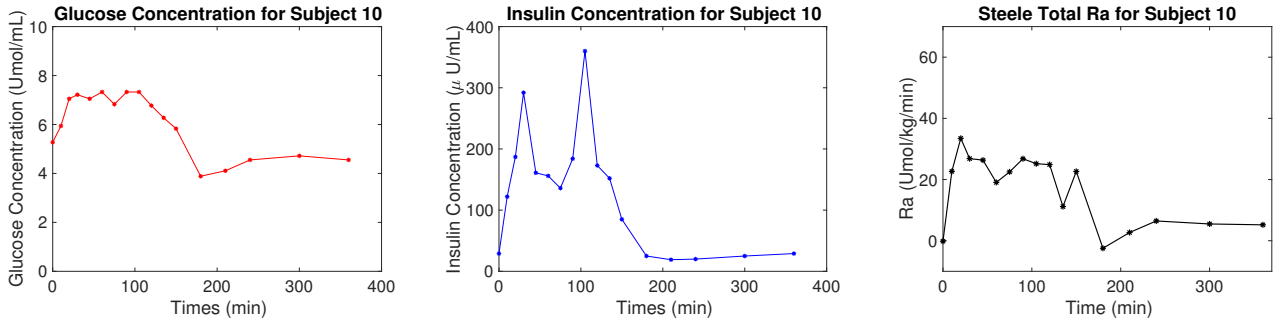

Figure 6.1: Glucose concentration, insulin concentration and Steele's total Ra for Subject 10.

For Subject 10, blood glucose concentrations (Figure 6.1(a)) stayed elevated for the first 105 minutes following drink ingestion which caused a double peak in insulin concentration (Figure 6.1(b)). The second peak in insulin eventually drove glucose levels down to baseline levels. Total Ra (Figure 6.1(c)) is consistent with the glucose profile: it remains elevated while glucose is high, decreases with glucose, and then comes back up to return to baseline.

Subject 12 shows an initial high glucose peak followed by a much smaller peak (Figure 6.2(a)) with corresponding insulin (Figure 6.2(b)) peaking twice: a high peak early on and then a smaller peak around 2 hours to push glucose levels back down to baseline.

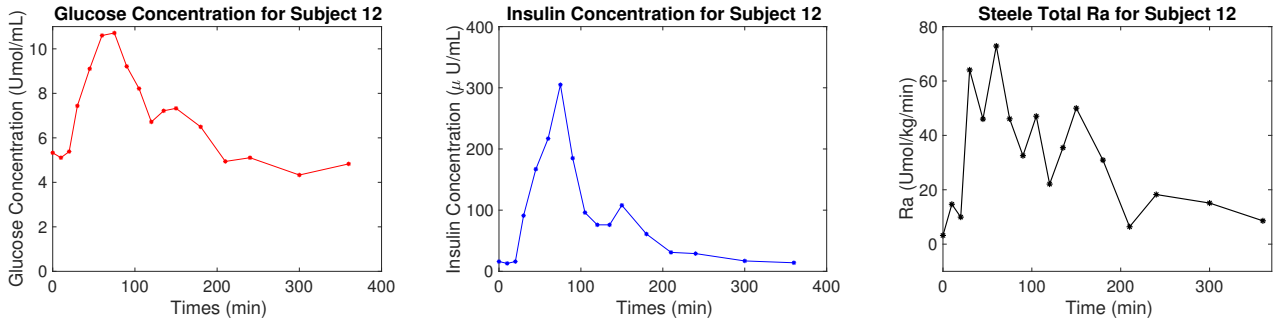

Figure 6.2: Glucose concentration, insulin concentration and Steele's total Ra for Subject 12.

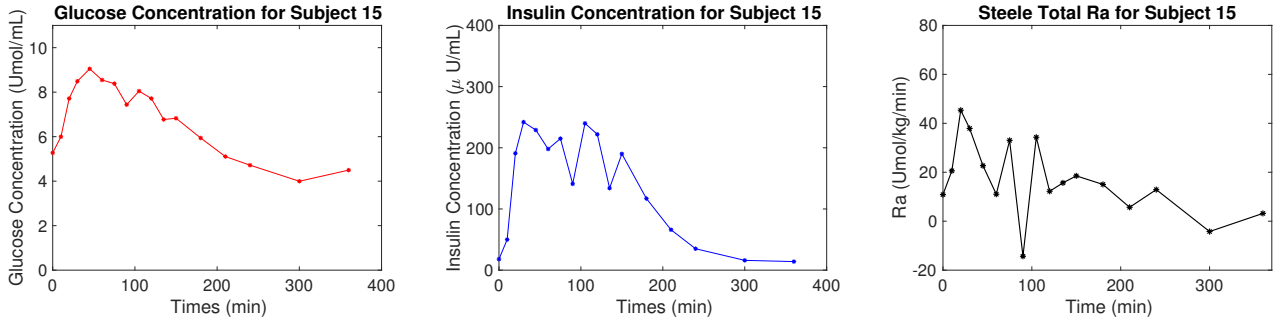

Figure 6.3: Glucose concentration, insulin concentration and Steele's total Ra for Subject 15.

The glucose concentration profile of Subject 15 (Figure 6.3(a)) peaks around 45 minutes post-drink but glucose levels remained elevated over the course of 2.5 hours. In response, insulin (Figure 6.3(b)) peaked repeatedly before effectively reducing the glucose concentration.

Overlapping all four Ra_{exo} methods for Subject 10 (Figure 6.5(a)) shows that all methods peak at the same time post-drink although they have different amplitudes in the earlier stage of the OGTT protocol. The methods also return to baseline at the same time. Similar behavior is observed in the computed Ra_{endo} values (Figure 6.5(b)) where the peaks vary in amplitude but all methods predict very similar values of Ra_{endo} after 2.5 hours.

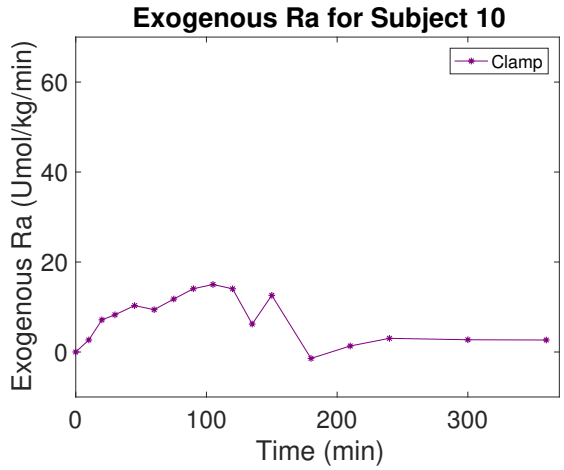

(a) Clamp Model

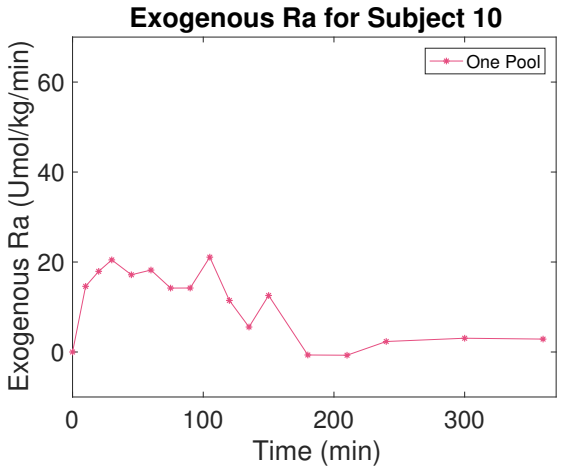

(b) One Pool

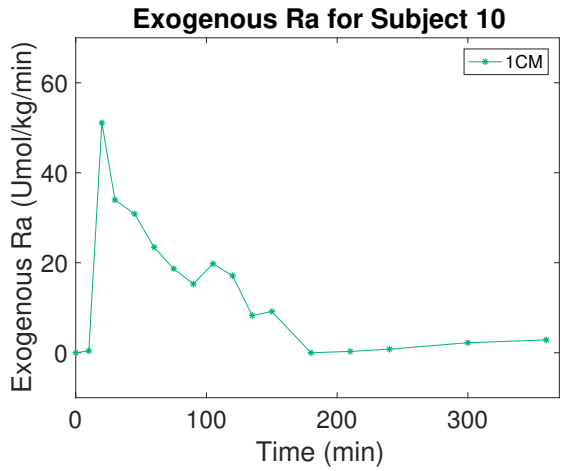

(c) 1CM

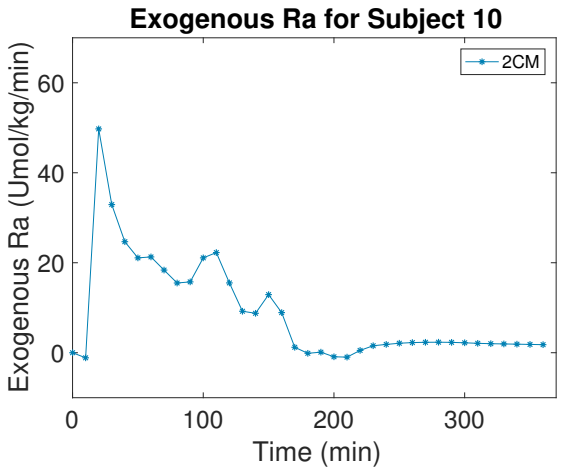

(d) 2CM

Figure 6.4: Ra_{exo} computed with (a) the Clamp Model, (b) the One Pool Model, (c) the One Compartment Model and (d) the Two Compartment Model for Subject 10.

The Ra_{exo} estimates vary greatly in magnitude for Subject 12 (Figure 6.7(a)). The more extreme values shown by the One and Two Compartment methods may indicate measurement error in the glucose tracer data for this subject.

Consistent with the results for Subjects 10 and 12, Ra_{exo} and Ra_{endo} estimates for Subject 15 show peaks at roughly the same time but with different amplitudes. However, there is more variability among the methods towards the end of the OGTT protocol (see Figure 6.9).

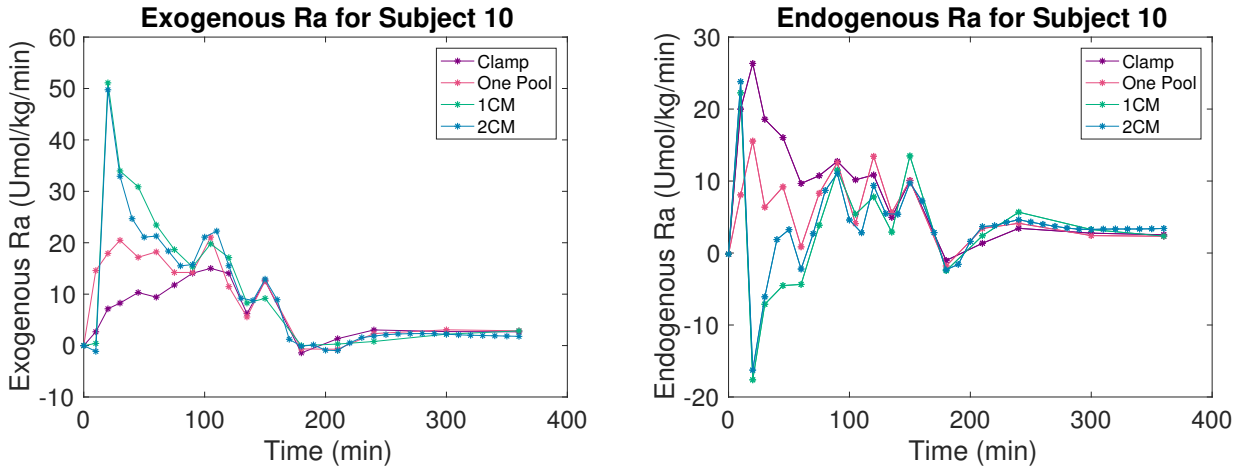

Figure 6.5: The calculated Ra_{exo} and the corresponding Ra_{endo} for each method for Subject 10.

For Subject 10, Figure 6.10, Figure 6.11, Figure 6.12 and Figure 6.13 show that RM run with the Clamp model did a better job of capturing the behavior of total glucose but RM* run with the One Pool method was better for approximating meal glucose. The same is true for Subject 12: the Clamp and One Pool methods more accurately approximated total and meal glucose, respectively, when run in RM and RM* (see Figure 6.14 and Figure 6.15). The glucose profile of Subject 15 proved to be more difficult for all Ra_{exo} methods. RM run with the One Pool method produced, comparatively, the most accurate results but it underestimates total glucose during the first 2 hours (see Figure 6.19).

Table 6.1: Estimates of S_I^{ref} and S_I^{*ref} for Subject 10

Method	S_I^{ref}	S_I^{*ref}
Clamp	5.13e-02	6.54e-03
One Pool	1.79e-07	3.72e-03
One Compartment	1.00e-08	1.34e-02
Two Compartment	4.56e-08	4.48e-03

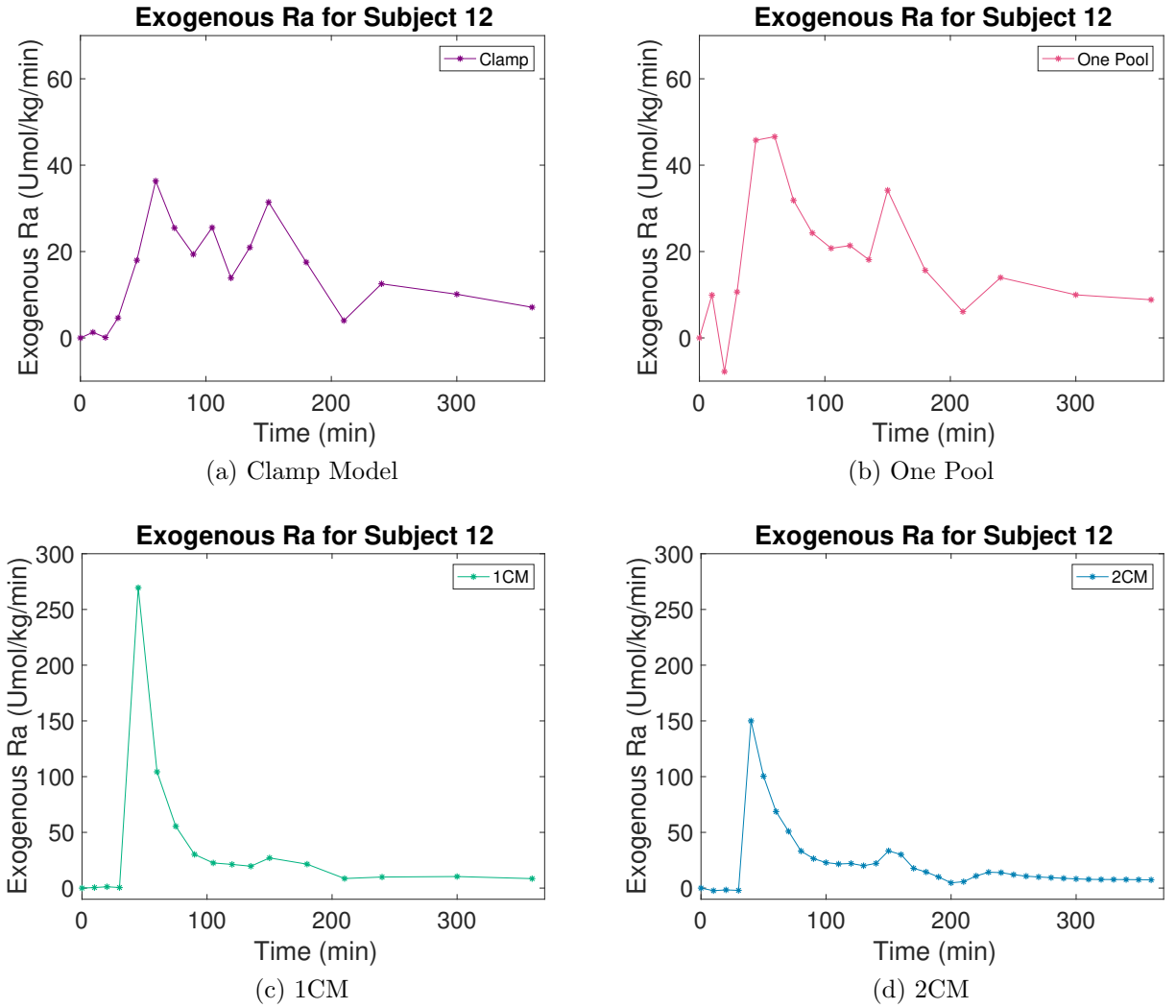

(a) Clamp Model (b) One Pool

(c) 1CM (d) 2CM

Figure 6.6: Ra_{exo} computed with (a) the Clamp Model, (b) the One Pool Model, (c) the One Compartment Model and (d) the Two Compartment Model for Subject 12.

Table 6.2: Estimates of S_I^{ref} and S_I^{*ref} for Subject 12

Method	S_I^{ref}	S_I^{*ref}
Clamp	5.16e+03	3.75e-03
One Pool	7.68e-08	7.85e-01
One Compartment	2.56e-05	9.16
Two Compartment	8.68e-11	4.11

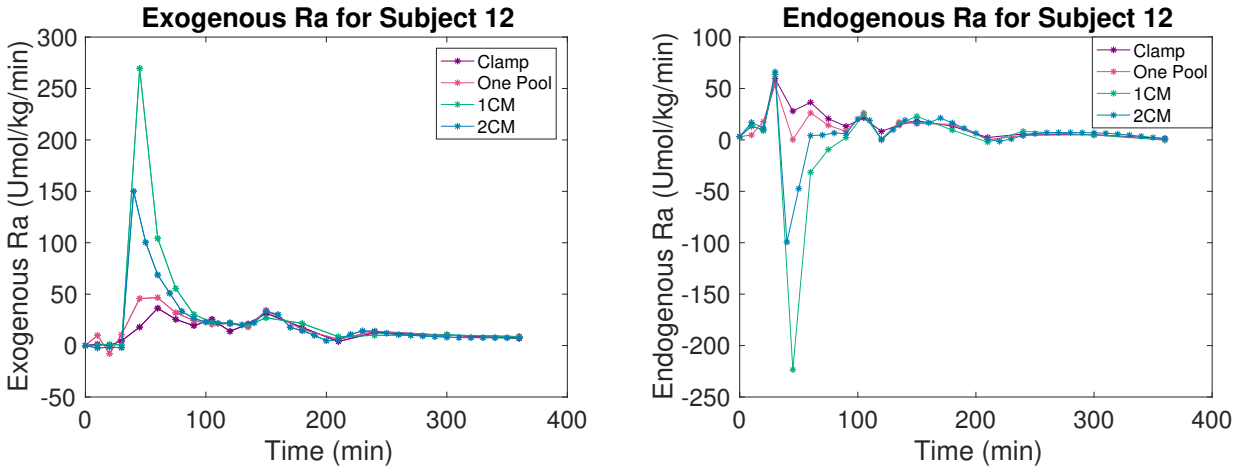

Figure 6.7: The calculated Ra_{exo} and the corresponding Ra_{endo} for each method for Subject 12.

Table 6.3: Estimates of S_I^{ref} and S_I^{*ref} for Subject 15

Method	S_I^{ref}	S_I^{*ref}
Clamp	5.68e-06	6.70e-03
One Pool	4.35e+02	1.39e-02
One Compartment	1.52e-09	1.77
Two Compartment	1.55e-07	1.66e-06

Table 6.1, Table 6.2, and Table 6.3, show S_I^{ref} and S_I^{*ref} estimates from RM and RM* for each method and each subject. For Subject 10, the S_I^{*ref} estimates are much larger for the One Pool, One and Two Compartment methods. The S_I^{*ref} estimate produced by the Clamp model are smaller than the estimate of S_I^{ref}. Subject 12 shows a similar pattern in that S_I^{*ref} estimates are much larger for the last three methods but the S_I^{ref} computed with the Clamp model is significantly larger than the S_I^{*ref} estimate. The S_I^{ref} and S_I^{*ref} estimates of Subject 15 do not follow the same pattern: S_I^{*ref} estimates calculated from the Clamp, One and Two Compartment methods are bigger than S_I^{ref} estimates.

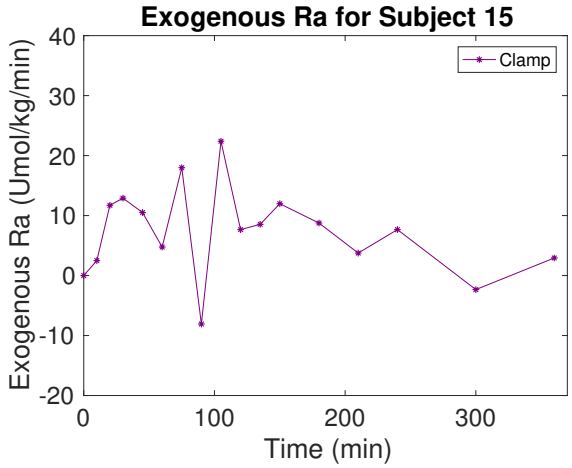

(a) Clamp Model

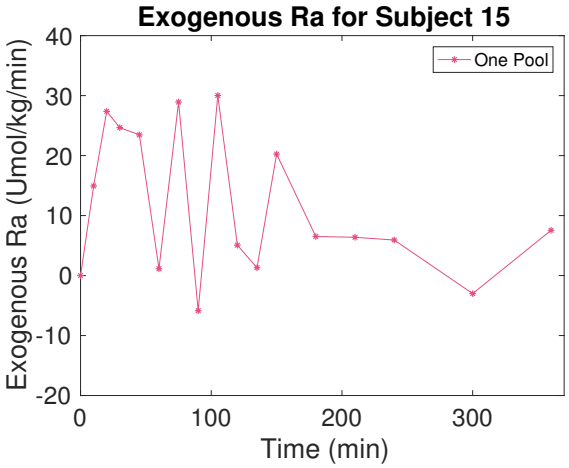

(b) One Pool

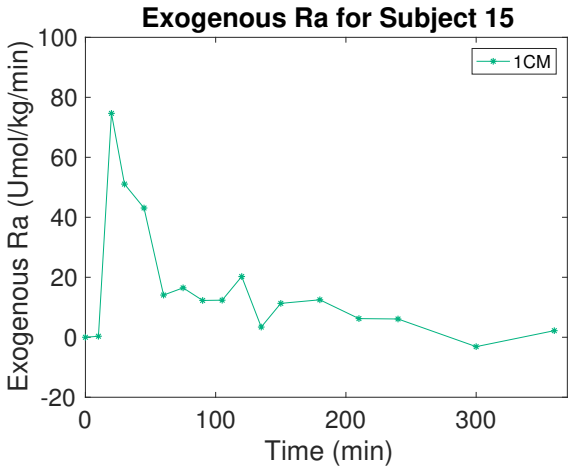

(c) 1CM

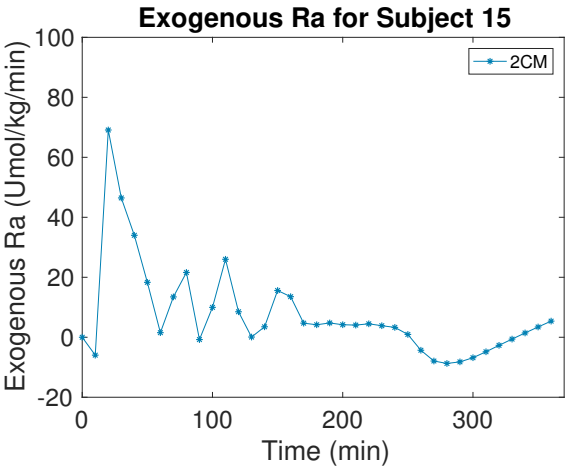

(d) 2CM

Figure 6.8: Ra_{exo} computed with (a) the Clamp Model, (b) the One Pool Model, (c) the One Compartment Model and (d) the Two Compartment Model for Subject 15.

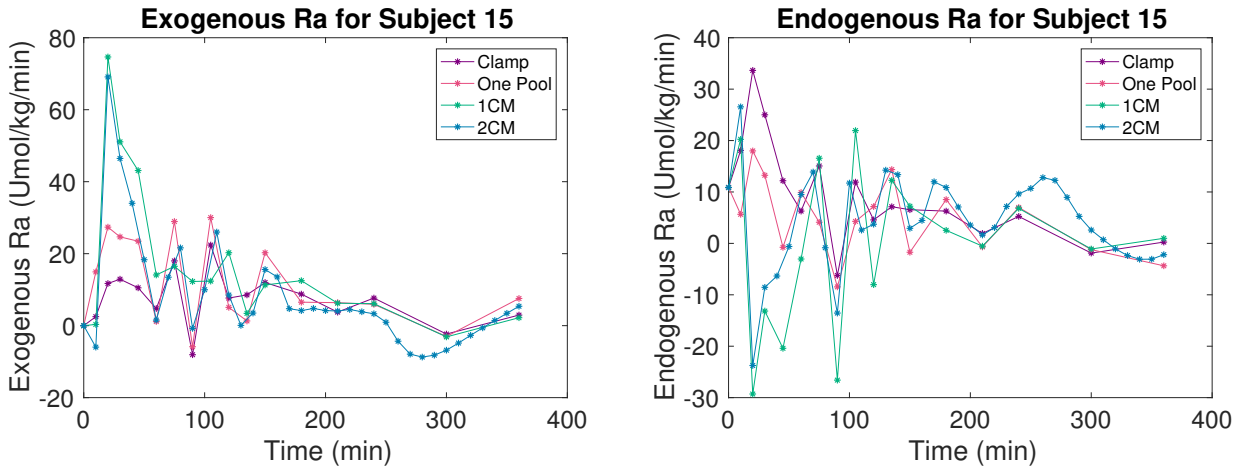

Figure 6.9: The calculated Ra_{exo} and the corresponding Ra_{endo} for each method for Subject 15.

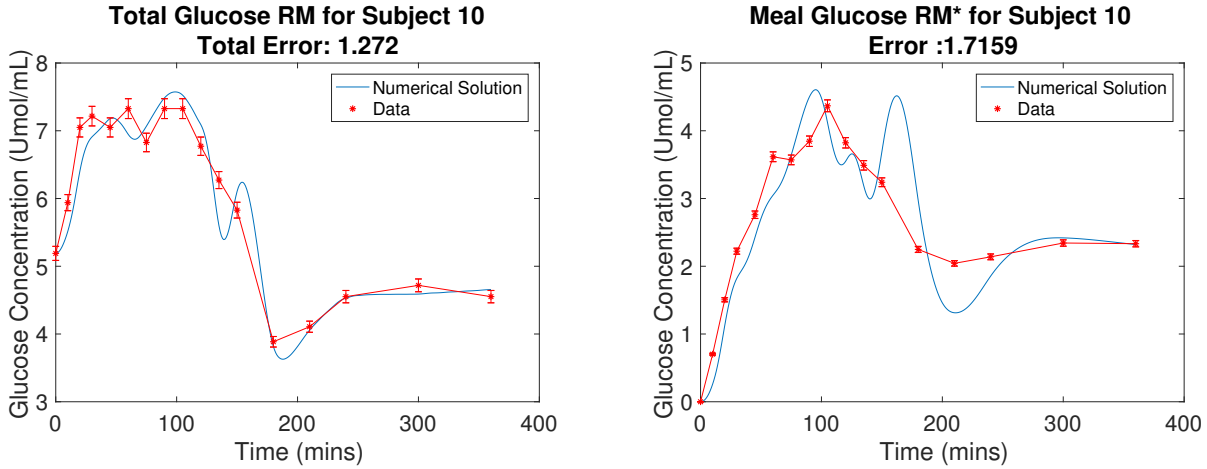

Figure 6.10: RM and RM* computed with the Clamp Model for Subject 10.

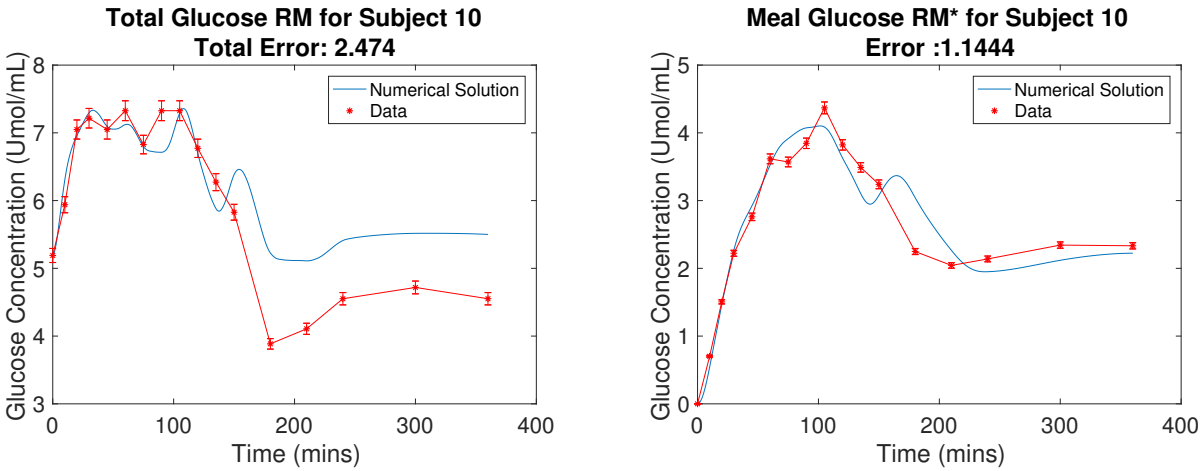

Figure 6.11: RM and RM* computed with the One Pool Model for Subject 10.

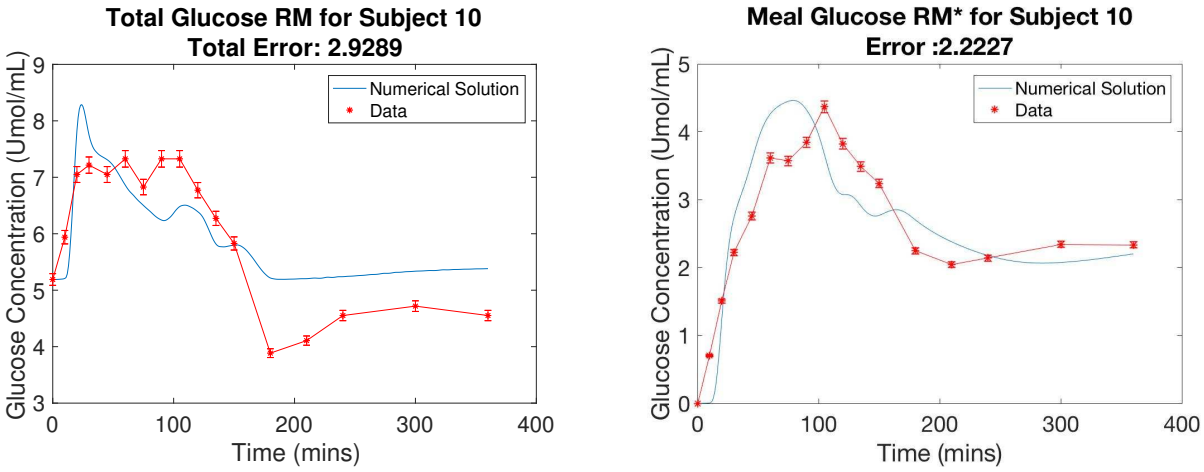

Figure 6.12: RM and RM* computed with the One Compartment Model for Subject 10.

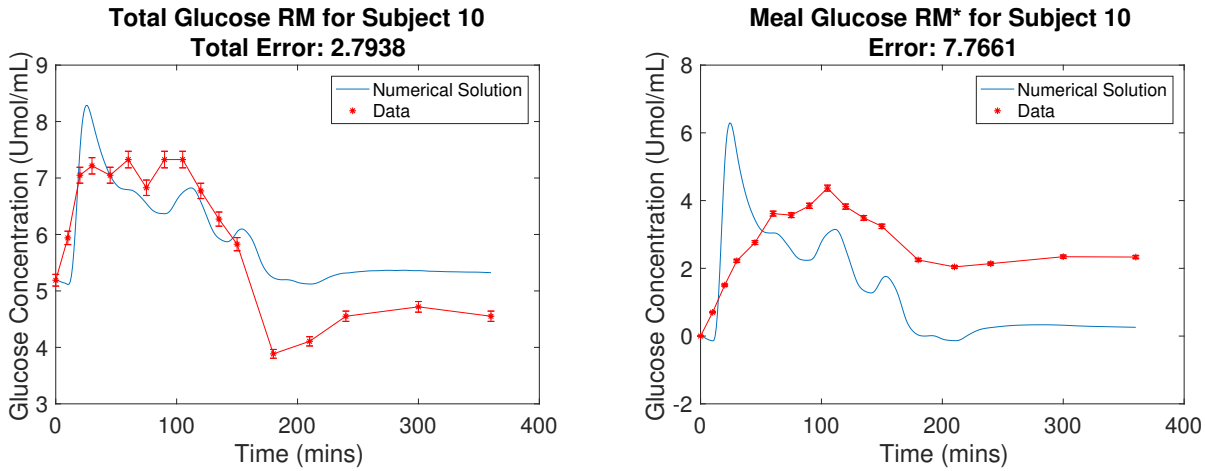

Figure 6.13: RM and RM* computed with the Two Compartment Model for Subject 10.

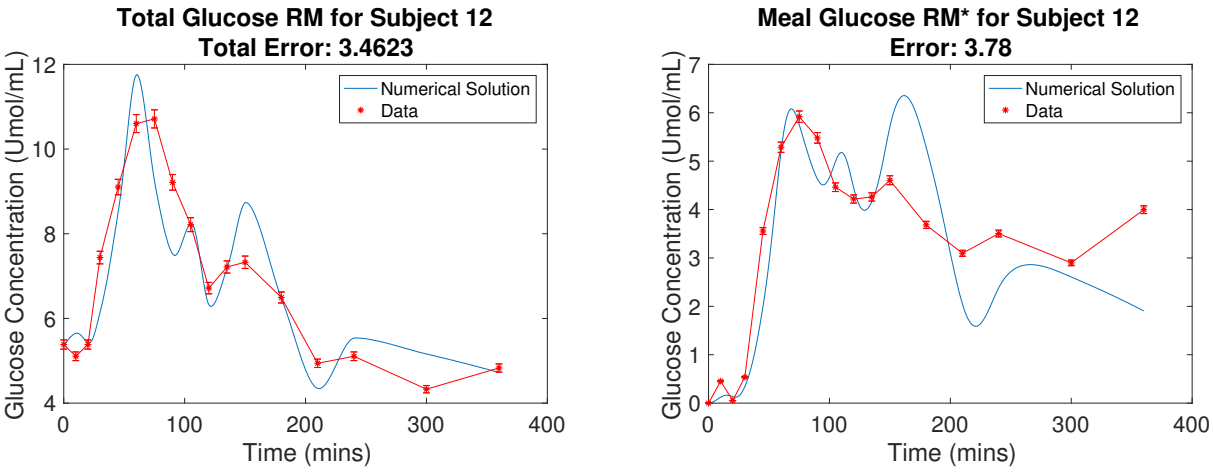

Figure 6.14: RM and RM* computed with the Clamp Model for Subject 12.

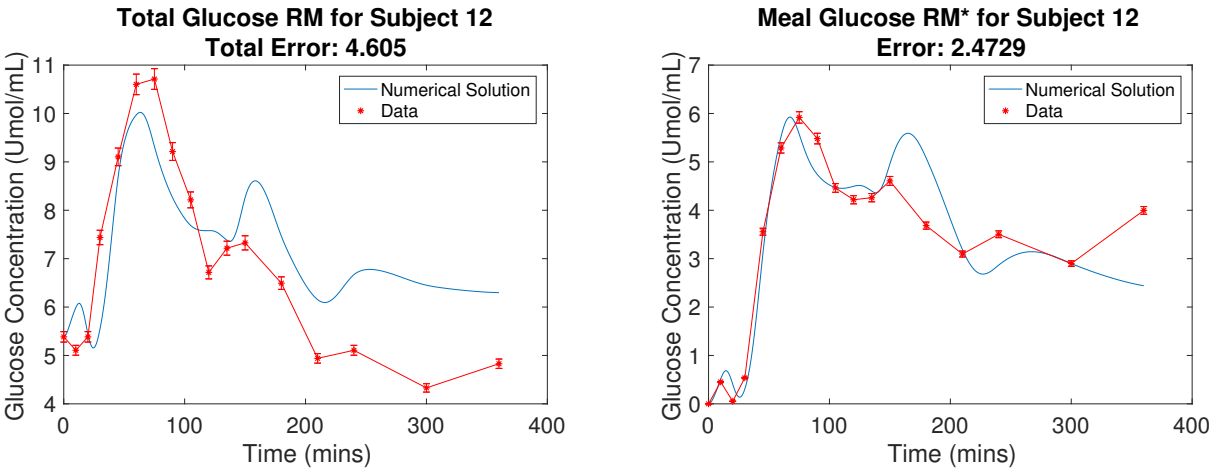

Figure 6.15: RM and RM* computed with the One Pool Model for Subject 12.

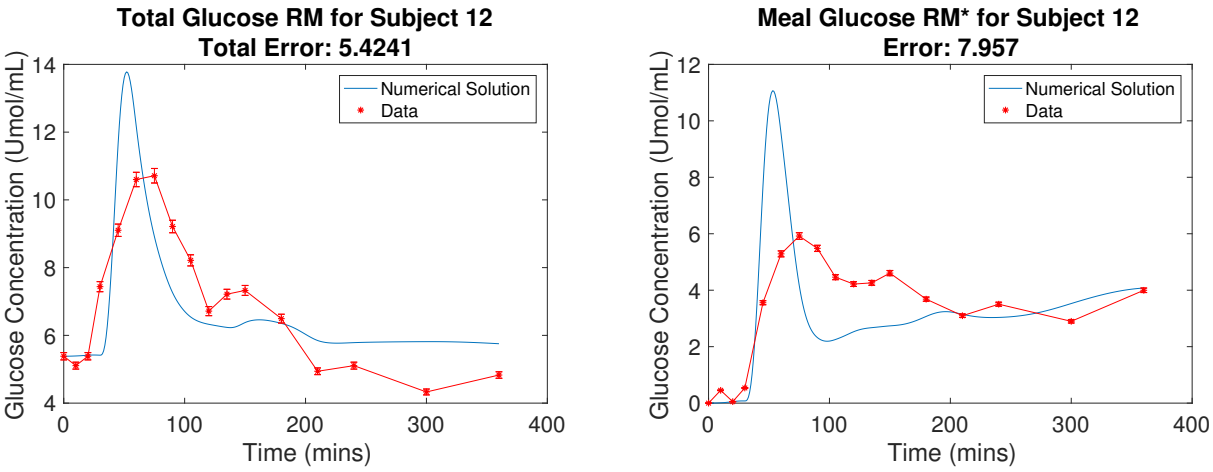

Figure 6.16: RM and RM* computed with the One Compartment for Subject 12.

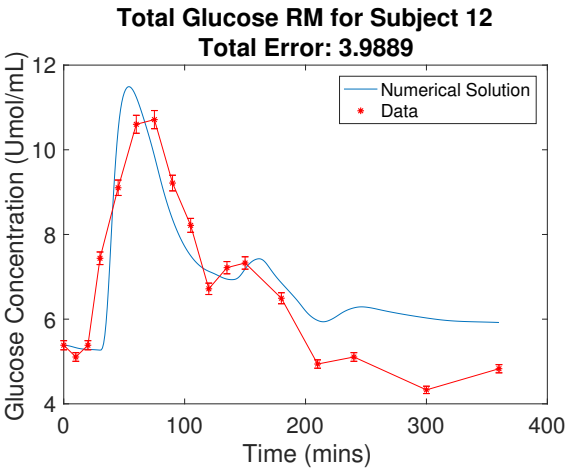

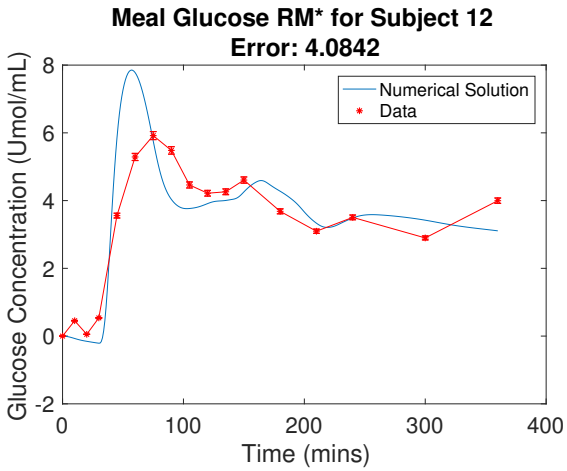

Figure 6.17: RM and RM* computed with the Two Compartment for Subject 12.

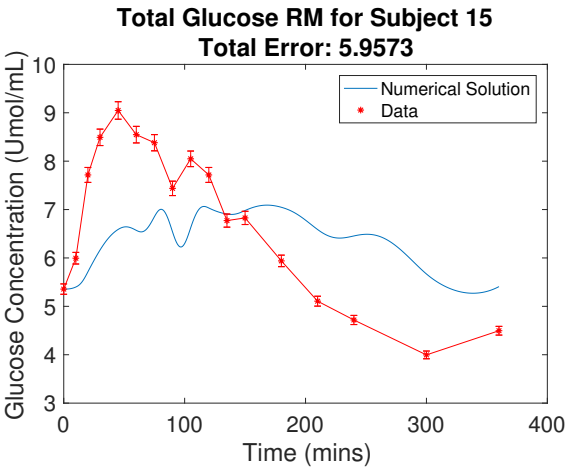

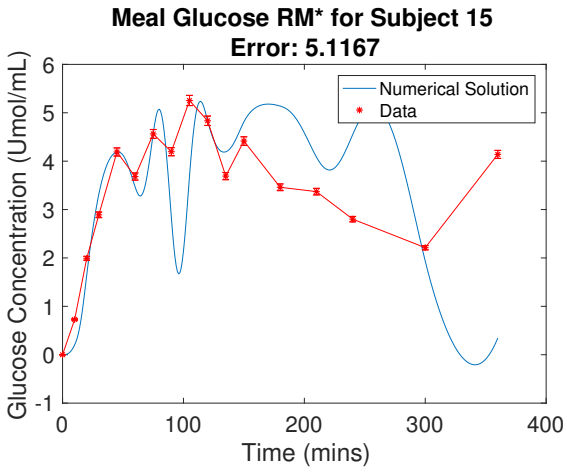

Figure 6.18: RM and RM* computed with the Clamp Model for Subject 15.

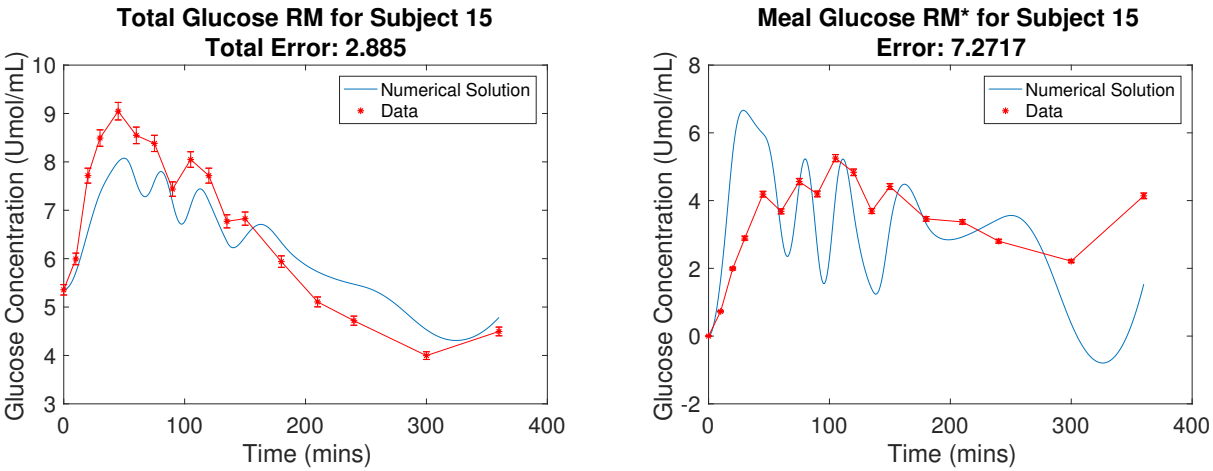

Figure 6.19: RM and RM* computed with the One Pool Model for Subject 15.

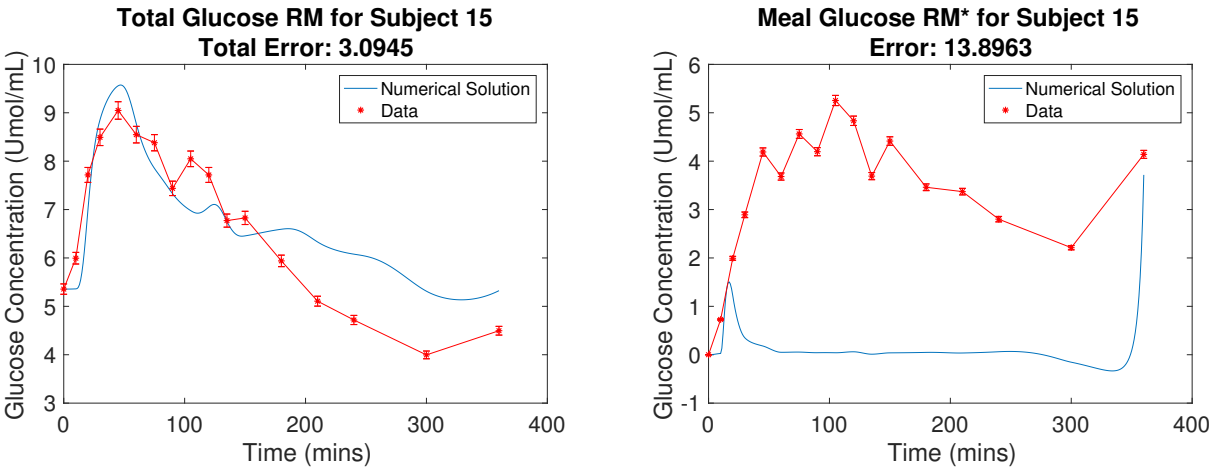

Figure 6.20: RM and RM* computed with the One Compartment Model for Subject 15.

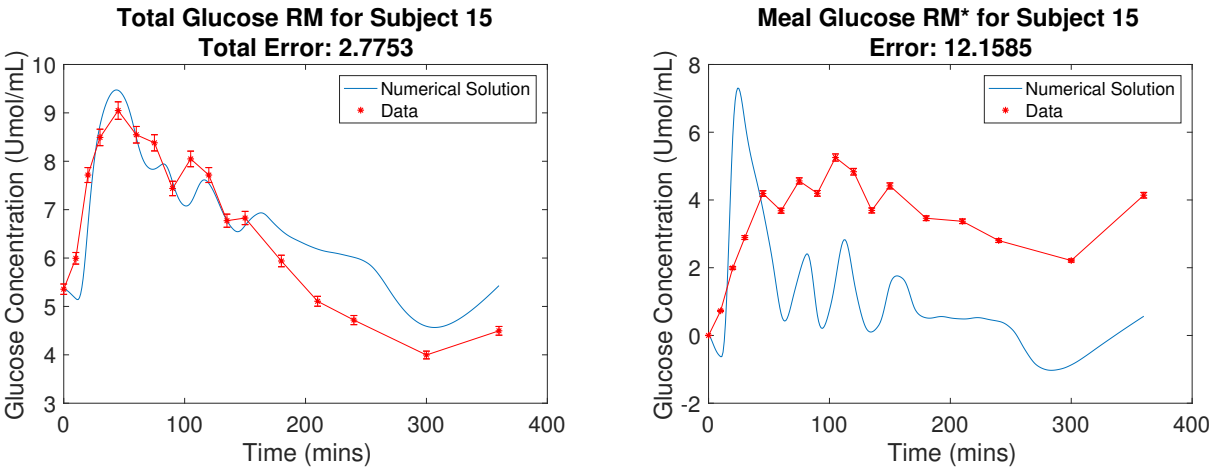

Figure 6.21: RM and RM* computed with the Two Compartment Model for Subject 15.

CHAPTER 7
CONCLUSION

The objective of this project was to determine how each method for computing Ra_{exo} impacts estimates of S_I and S_I^*. The implementation and results of four published methods for computing Ra_{exo} were analyzed, and these estimates were used in the differential equations-based models OMM and OMM*. From these models of glucose dynamics, S_I and S_I^* were calculated for each method and subject.

All of the methods for computing Ra_{exo} peak at similar times, and the greatest variability among estimates of Ra_{exo} occurs in the first ≈ 90 minutes following ingestion of the test drink. This corresponds to the time period where the ratio of tracer I to tracer II changes rapidly. The One Compartment and Two Compartment models explicitly involve the ratio of tracer II to tracer I, so they are more sensitive to the changing ratios of the experiment compared to the Clamp and One Pool methods. This may account for the increased peak height observed in the One and Two Compartment models.

The total rate of appearance of glucose includes both exogenous and endogenous contributions so, physiologically, total Ra should always be greater than Ra_{exo}. Since total Ra is defined to be the sum of Ra_{exo} and Ra_{endo} each method for computing Ra_{exo} predicts varying rates and degrees of suppression of Ra_{endo}. For some methods this leads to predictions of non-physiologic negative Ra_{endo} values. These non-physiologic Ra_{endo} values may be due to underestimates of Ra_{exo} associated with steady state assumptions that are not appropriate for these non-steady state conditions [19].

There are limitations associated with each method. The Clamp and One Pool model both use total Ra to calculate Ra_{exo}. This may introduce errors in Ra_{exo} due to known errors associated with computing Ra using Steele's non-steady state equation [19]. Specifically, the change in enrichment must be estimated and the fraction of the glucose pool that behaves as a rapidly mixing pool is assumed [10]. The latter limitation is common to all models and is discussed in more detail below. Additionally, the Clamp model assumes the ratio of E_P to E_D is fixed for each time interval and computes Ra_{exo} as a proportion of total Ra based on this ratio. Since E_P actually changes over each time interval, this issue is most relevant soon after drink ingestion when E_P is changing quickly.

Although the One and Two Compartment models do not rely on computing total Ra, they apply Steele's non-steady state equation to labeled glucose. To minimize the non-steady state error, a third tracer with variable infusion may be used. This strategy seeks to keep the ratio of tracer II to tracer I more or less constant such that steady state conditions can be mimicked [19]. However, this method may introduce additional error because the role of endogenous glucose production must be assumed and this role may not be accurate for all participants. Although there have been tracer infusion profiles developed for some populations [19], tracer infusion profiles may be more variable in populations with IR such as obese adolescent females. Ideally tracer infusion profiles should be individualized, but this is rarely feasible.

A common limitation among all of the methods is the assumption of a fixed volume of distribution for glucose. Studies suggest that the blood glucose pool where mixing occurs grows with time following an OGTT or a meal. A limitation of using Steele's equation for total Ra in calculations of glucose kinetics is the necessity of assuming a parameter p to account for imperfect mixing in the glucose pool. Different approaches have been applied to find the most accurate value of the volume of distribution to use in Steele's equation,

but there is no one number that gives correct calculations of total Ra in all circumstances [10, 1]. Proposed volumes of distribution range from 40 $mL \cdot kg^{-1}$ to 200 $mL \cdot kg^{-1}$. Ra was more accurately computed in the early stages of an OGTT or IVGTT with 40 $mL \cdot kg^{-1}$. However, as the enrichment of plasma glucose reached a new equilibrium, changes in this enrichment reflected a much larger volume of distribution, closer to 200 $mL \cdot kg^{-1}$ [10].

The S_I^{ref} and S_I^{*ref} estimates are highly sensitive to the chosen Ra_{exo} method. Previously published results show that S_I and S_I^* should be on the order of $10^{-2}\, mL \cdot kg^{-1} \cdot min^{-1}$ per $\mu U \cdot mL^{-1}$ [12, 7]. The calculated estimates show this is the case for a few of the S_I^{ref} and S_I^{*ref} estimates but the order of magnitudes for most of the estimates are very different from this benchmark. However, the S_I and S_I^* values reported here reflect estimates using RM and RM*. The full implementation of OMM/OMM* requires estimating S_I and S_I^* with FM. Although these estimates will depend on the parameter values fixed from the RM/RM* computation, the sensitivity of FM-based estimates of S_I and S_I^* to the methods used to estimate Ra_{exo} is not known. Future work will investigate this dependence and the implications for model-dependence in estimates of insulin sensitivity.

True Ra_{exo} cannot be directly measured without extremely invasive experiments that cannot be performed in humans [1]. However, this work has established that different methods for computing Ra_{exo} give rise to different estimates of insulin sensitivity (S_I and S_I^*) when applied to RM and RM*. Clearly, this model-dependence represents a major challenge for quantification of insulin sensitivity. Future work is needed to establish methodologies for robustly estimating Ra_{exo} and insulin sensitivity using data from dual-tracer OGTT protocols.

REFERENCES CITED

[1] Allsop, J. R., Wolfe, R. R., and Burke, J. F. The reliability of rates of glucose appearance in vivo calculated from constant tracer infusions. *Biochemical Journal 172*, 3 (1978), 407–416.

[2] Azziz, R. Evaluation for insulin resistance and comorbidities related to insulin resistance in polycystic ovary syndrome. In *Insulin Resistance and Polycystic Ovarian Syndrome: Pathogenesis, Evaluation and Treatment*, E. Diamanti-Kandarakis, J. E. Nestler, D. Panidis, and R. Pasquali, Eds. Humana Press, 99 Riverview Drive, Suite 208, Totowa, New Jersey 07512, 2007, pp. 1–14.

[3] Basu, R., Camillo, B. D., Toffolo, G., Basu, A., Shah, P., Vella, A., Rizza, R., and Cobelli, C. Use of a novel triple-tracer approach to assess postprandial glucose metabolism. *Endocrinology and Metabolism - American Journal of Physiology 284* (2003), 55–69.

[4] Bergman, B., Howard, D., Schauer, I., Maahs, D., Snell-Bergeon, J., Clement, T., Eckel, R., Perreault, L., and Rewers, M. The importance of palmitoleic acid to adipocyte insulin resistance and whole-body insulin sensitivity in type 1 diabetes. *J Clin Endocrinol Metab 98* (2013), E40–50.

[5] Bergman, B. C., Howard, D., Schauer, I. E., Maahs, D. M., Snell-Bergeon, J. K., Eckel, R. H., Perreault, L., and Rewers, M. Features of hepatic and skeletal muscle insulin resistance unique to type 1 diabetes. *J Clin Endocrinol Metab 97* (2012), 1663–1672.

[6] Bergman, R. N., Phillips, L. S., and Cobelli, C. Physiologic evaluation of factors controlling glucose tolerance in man: Measurement of insulin sensitivity and β-cell glucose sensitivity from the response to intravenous glucose. *Journal of Clinical Investigation 68* (1981), 1456– 1467.

[7] Cobelli, C., Man, C. D., Mariatoffolo, G., Basu, R., Vella, A., and Rizza, R. The oral minimal model method. *Diabetes 63* (2014), 1203–13.

[8] Gilker, C. D., Pesola, G. R., and Matthews, D. A mass spectrometric method for measuring glycerol levels and enrichments in plasma using 13c and 2h stable isotopic tracers. *Anal Biochem 205* (1992), 172–178.

[9] Ha, J., Satin, L. S., and Sherman, A. S. A mathematical model of the pathogenesis, prevention, and reversal of type 2 diabetes. *Endocrinology 157* (2015), 625 – 635.

[10] Kim, I.-Y., Williams, R. H., Schutzler, S. E., Lasley, C. J., Bodenner, D. L., Wolfe, R. R., and Coker, R. H. Acute lysine supplementation does not improve hepatic or peripheral insulin sensitivity in older, overweight individuals. *Nutrition & Metabolism 11.1* (2014), 1–8.

[11] Lindquist, K. A., Chow, K., West, A., Pyle, L., Isbell, T., Cree-Green, M., and Nadeau, K. The statstrip glucose monitor is suitable for use during hyperinsulinemic euglycemic clamps in a pediatric population. *Diabetes Technology & Therapeutics* (2014).

[12] Man, C. D., Caumo, A., Basu, R., Rizza, R., Toffolo, G., and Cobelli, C. Minimal model estimation of glucose absorption and insulin sensitivity from oral test: validation with a tracer method. *Endocrinology and Metabolism - American Journal of Physiology 287* (2004), 637–643.

[13] Man, C. D., Caumo, A., Basu, R., Rizza, R., Toffolo, G., and Cobelli, C. Measurement of selective effect of insulin on glucose disposal from labeled glucose oral test minimal model. *American Journal of Physiology - Endocrinology and Metabolism 289* (2005), 909–914.

[14] Man, C. D., Caumo, A., and Cobelli, C. The oral glucose minimal model: Estimation of insulin sensitivity from a meal test. *IEEE Transactions on Biomedical Engineering 49.5* (2002), 419–429.

[15] Mari, A. Estimation of the rate of appearance in the non-steady state with a two-compartment model. *American Journal of Physiology-Endocrinology and Metabolism 263*, 2 (1992), 400–415.

[16] Marks, V. Metabolism and maintenance of blood glucose level. In *Encyclopedia of Human Nutrition*, B. Caballero, Ed., 3 ed., vol. 2. Elsevier Ltd, Radarweg 29, PO Box 211, 1000 AE Amsterdam, The Netherlands, 2013, pp. 1–14.

[17] Moran, A., David R. Jacobs, J., Steinberger, J., Hong, C.-P., Prineas, R., Luepker, R., and Sinaiko, A. R. Insulin resistance during puberty: results from clamp studies in 357 children. *Diabetes 48*, 10 (1999), 2039–2044.

[18] Proietto, J. Estimation of glucose kinetics following an oral glucose load. *Hormone and Metabolic Research Supplement Series* (1990), 25 – 30.

[19] Rizza, R., Toffolo, G., and Cobelli, C. Accurate measurement of postprandial glucose turnover: Why is it difficult and how can it be done (relatively) simply? *Diabetes 65* (2016), 1133–1145.

[20] Steele, R. Influences of glucose loading and of injected insulin on hepatic glucose output. *Annals of the New York Academy of Sciences* (1959).

[21] Vahidi, O., Kwok, K. E., Gopaluni, R. B., and Knop, F. K. A comprehensive compartmental model of blood glucose regulation for healthy and type 2 diabetic subjects. *Medical & Biological Engineering & Computing 54* (2016), 1383 – 1398.

[22] Wolfe, R. R., and Chinkes, D. *Isotope tracers in metabolic research: principles and practice of kinetic analysis*. John Wiley & Sons, 2005.